Quadratic Jahn-Teller effect of fullerene anions

Dan Liu,[1] Yasuyuki Niwa,[2,*] Naoya Iwahara,[1,†] Tohru Sato,[3,4,5] and Liviu F. Chibotaru[1,‡]

[1]*Theory of Nanomaterials Group, University of Leuven, Celestijnenlaan 200F, B-3001 Leuven, Belgium*

[2]*Undergraduate School of Industrial Chemistry, Faculty of Engineering, Kyoto University, Kyoto 606-8501, Japan*

[3]*Fukui Institute for Fundamental Chemistry, Kyoto University, Takano-Nishihiraki-cho 34-4, Sakyo-ku, Kyoto 606-8103, Japan*

[4]*Department of Molecular Engineering, Graduate School of Engineering, Kyoto University, Kyoto 615-8510, Japan*

[5]*Unit of Elements Strategy Initiative for Catalysts & Batteries, Kyoto University, Katsura, Nishikyo-ku, Kyoto 615-8510, Japan*

(Received 21 May 2018; published 2 July 2018)

The quadratic Jahn-Teller effect of C_{60}^{n-} ($n = 1$–5) is investigated from the first principles. Employing the density functional theory calculations with hybrid functional, the quadratic vibronic coupling constants of C_{60}^{-} were derived. The warping of the adiabatic potential energy surface of C_{60}^{-} by the quadratic vibronic coupling is estimated to be about 2 meV, which is much smaller than the Jahn-Teller stabilization energy ($\approx$ 50 meV). Because of the selection rule and the vibronic reduction, the quadratic coupling slightly modifies the vibronic states of C_{60} anions. Particularly, in the case of C_{60}^{3-}, parity and symmetry selection rule significantly reduces the effect of quadratic coupling on vibronic states. The present results confirm that the low-energy vibronic dynamics of C_{60}^{n-} is of pseudorotational type.

DOI: 10.1103/PhysRevB.98.035402

I. INTRODUCTION

The Jahn-Teller (JT) effect [1–3] plays a central role in the low-energy structures of fullerene C_{60} anions and the electronic properties of fullerene-based compounds. The relative importance of the static and dynamical JT effect has been intensively investigated in molecular spectroscopy [4–14], in the superconducting and insulating alkali-doped fullerides [15–33], in the ferromagnetic TDAE-C_{60} [34,35], where TDAE stands for tetrakis(dimethylamino)ethylene, and other organic fullerene compounds [36–38]. The dynamical $t_{1u}^n \otimes h_g$ JT model for C_{60}^{n-} ions has been analyzed with various approaches. Within a linear vibronic model, the vibronic dynamics is of pseudorotational type [17,19], while, by turning on the quadratic vibronic coupling, it becomes of tunneling splitting type [39,40] due to the hindering of pseudorotation.

To assess the nature of the JT effect in C_{60} anions, knowledge of vibronic coupling constants is essential. After many experimental [6,9,20] and theoretical [41–49] studies, the linear orbital vibronic coupling parameters of C_{60}^{-} were finally established recently [10] (for details on this problem, see Refs. [10,50]). In this work, the linear vibronic coupling parameters were derived by simulating the high-resolution photoelectron spectrum [51], and the obtained parameters were found to agree well with density functional theory (DFT) calculations using a hybrid functional. Subsequent calculations within the *GW* approximation gave close values of stabilization energy for C_{60}^{-} [52]. On the other hand, knowledge of nonlinear vibronic coupling parameters of C_{60} anions is still lacking. Because of intermediate linear vibronic coupling in C_{60}^{-} [10], the quadratic coupling is expected to be weak [26]. Indeed, the photoelectron spectra of C_{60}^{-} [6,10] and infrared (IR) spectra of Mott-insulating Cs_3C_{60} [33] have been well reproduced without quadratic JT coupling. On the other hand, near-IR spectra [7–9] of C_{60} anions and electron paramagnetic resonance measurements of C_{60}^{-} in solution [14] have been interpreted on the basis of the tunneling splitting character of the low-lying vibronic spectrum.

The purpose of this work is to reveal the nature of the JT dynamics of C_{60}^{n-}, including both linear and quadratic vibronic coupling. The quadratic vibronic coupling constants of C_{60} anions were derived from the DFT calculations with the B3LYP functional. With the obtained constants, the warping of the adiabatic potential energy surface of C_{60}^{-} was found to amount to a few meV, which is much smaller than the JT stabilization energy. It was also found that, because of the selection rule and the vibronic reduction, the quadratic coupling does not modify the vibronic spectrum of the linear $t_{1u}^n \otimes 8h_g$ JT model. The present results show that the quadratic vibronic coupling in C_{60} anions is sufficiently weak for the JT dynamics to remain of pseudorotational type.

II. QUADRATIC JAHN-TELLER MODEL FOR C_{60} ANIONS

A. Bielectronic and vibronic interactions

The neutral fullerene C_{60} (I_h symmetry) has triply degenerate t_{1u} lowest unoccupied molecular orbitals (LUMOs). The LUMO levels are well separated from the other molecular orbital levels, therefore the t_{1u} shell model describes adequately the low-energy electronic structure of C_{60}^{n-} anions ($n = 1$–5). The model Hamiltonian for the C_{60}^{n-} ion consists of the bielectronic term $\hat{H}_{\rm bi}$ and the vibronic term. The former causes

*Present address: Institute for Chemical Research, Kyoto University, Uji, Kyoto 611-0011, Japan.

†naoya.iwahara@gmail.com

‡liviu.chibotaru@gmail.com

the term splitting of the t_{1u}^n configurations. The latter describes the vibronic coupling between the t_{1u} orbitals and the nuclear vibrations of a_g or h_g type [1]. Using the equilibrium structure of neutral C_{60} as a reference, the vibronic term is represented as the sum of the following contributions [3,17–19,39]:

$$\hat{H}_{\rm vib} = \sum_{\mu\Gamma\gamma} \frac{1}{2}\left(\hat{p}^2_{\Gamma(\mu)\gamma} + K^{\Gamma}_{\mu}\hat{q}^2_{\Gamma(\mu)\gamma}\right), \tag{1}$$

$$\hat{H}^{(1)}_{\rm JT} = \sum_{\lambda\lambda'\sigma}\sum_{\mu\gamma} V^{h_g}_{\mu}\hat{c}^{\dagger}_{\lambda\sigma}\hat{c}_{\lambda'\sigma}\hat{q}_{h_g(\mu)\gamma}\sqrt{\frac{5}{2}}\langle t_{1u}\lambda'|h_g\gamma t_{1u}\lambda\rangle, \tag{2}$$

$$\hat{H}^{(2)}_{\rm JT} = \sum_{\lambda\lambda'\sigma}\sum_{\mu_i\Gamma_i}\sum_{\nu\gamma} V^{\Gamma_1\Gamma_2}_{\nu\mu_1\mu_2}\hat{c}^{\dagger}_{\lambda\sigma}\hat{c}_{\lambda'\sigma} \times \{\hat{q}_{\Gamma_1(\mu_1)}\otimes\hat{q}_{\Gamma_2(\mu_2)}\}_{\nu h_g\gamma}\sqrt{\frac{5}{2}}\langle t_{1u}\lambda'|h_g\gamma t_{1u}\lambda\rangle. \tag{3}$$

Here, $\lambda = x,y,z$ and $\gamma = \theta,\epsilon,\xi,\eta,\zeta$ are the components of the t_{1u} and h_g irreducible representations of the I_h group, respectively, $\hat{q}$ and $\hat{p}$ are the mass-weighted normal coordinates and momenta of the reference system, respectively, μ denotes the vibrational modes of the same symmetry, $\{\hat{q}_{\Gamma_1}\otimes\hat{q}_{\Gamma_2}\}_{\nu h_g\gamma}$ are symmetrized products (for an explicit form, see Ref. [53]), $\langle t_{1u}\lambda'|h_g\gamma t_{1u}\lambda\rangle$ are the Clebsch-Gordan coefficients, and K^{Γ}, V^{Γ}, and $V^{\Gamma_1\Gamma_2}$ are the force constant and the linear and quadratic vibronic coupling parameters, respectively. The coefficient $\sqrt{5/2}$ is introduced in vibronic terms following Refs. [3,17–19,54,55], which results in $\sqrt{2/5}$ times smaller vibronic coupling parameters than those in Ref. [39]. As the basis of the h_g representation, atomic d functions are used [3,17–19,54,55]: θ, ϵ, ξ, η, and ζ components of the h_g representation transform as $(2z^2-x^2-y^2)/\sqrt{6}$, $(x^2-y^2)/\sqrt{2}$, $\sqrt{2}yz$, $\sqrt{2}zx$, and $\sqrt{2}xy$ components of the d orbitals, respectively, under symmetric operations of the I_h group (the Cartesian coordinate axes correspond to the C_2 axes of C_{60} as in Refs. [16,56,57]). Equation (3) contains two parameters [39] since the symmetric square of h_g contains two h_g ($\nu = 1,2$) [57]. The symmetrized polynomial $\{\hat{q}_{h_g(\mu_1)}\otimes\hat{q}_{h_g(\mu_2)}\}_{1h_g\gamma}$ and $\{\hat{q}_{h_g(\mu_1)}\otimes\hat{q}_{h_g(\mu_2)}\}_{2h_g\gamma}$ become zero for the deformation along the D_{3d} and D_{5d} minima, respectively, as in Ref. [39]. The vibronic Hamiltonian for the unimportant totally symmetric modes is not written here for simplicity.

It is convenient to write down the vibronic Hamiltonian in the basis of electronic terms, particularly when there is term splitting [3,19]. The orbital part for $C_{60}{}^{n-}$ can be written as follows:

$$\hat{H}^{(1)}_{\rm JT} = \sum_{\mu\gamma} V^{h_g}_{\mu}\hat{q}_{h_g(\mu)\gamma}\hat{C}^{(n)}_{\gamma}, \tag{4}$$

$$\hat{H}^{(2)}_{\rm JT} = \sum_{\mu_i\Gamma_i}\sum_{\nu\gamma} V^{\Gamma_1\Gamma_2}_{\nu\mu_1\mu_2}\{\hat{q}_{\Gamma_1(\mu_1)}\otimes\hat{q}_{\Gamma_2(\mu_2)}\}_{\nu h_g\gamma}\hat{C}^{(n)}_{\gamma}, \tag{5}$$

where $\hat{C}^{(n)}_{\gamma}$ are the matrices of the Clebsch-Gordan coefficients, which are given in Refs. [3,19] and also in the supplemental material [53]. For the derivation of the matrices in Eqs. (4) and (5) in the basis of t_{1u}^n terms, see Ref. [58].

B. Adiabatic potential energy surface

The structure of the adiabatic potential energy surface (APES) provides fundamental information about the nature of vibronic dynamics. According to Liehr's minimax rule [59], the JT distortion that lifts the degeneracy of the initial electronic state corresponds to the one maintaining the highest subgroup of the system. In the case of the I_h system with a T_{1u} electronic state ($n = 1,5$), the corresponding JT deformation is accordingly either of D_{5d} or of D_{3d} type. Further symmetry lowering may arise due to the higher-order vibronic coupling or pseudo-Jahn-Teller coupling [60]. The effect of the warping of the APES can be modeled using the invariants of the I_h group, which indeed shows the symmetry of the JT deformed structure either of D_{5d} or of D_{3d} [3]. This was unambiguously proved by explicitly analyzing the quadratic JT Hamiltonian [39]. The first ($\nu = 1$) and the second ($\nu = 2$) quadratic vibronic couplings in Eq. (3) favor the D_{5d} and D_{3d} deformations, respectively. If the energy difference between them is large, the system tends to be localized at the potential's minima.

So far, the analysis of the APES has been done only taking into account the JT active h_g mode [3,39,61,62]. However, in the case of the I_h system, the JT inactive modes can be included in Eq. (3). This is also understood based on subduction of irrep. Under $I_h \downarrow D_{5d}$, only the h_g representation contains the totally symmetric representation, whereas under $I_h \downarrow D_{3d}$ or $I_h \downarrow D_{2h}$, a totally symmetric representation also appears from the g_g representation [57]. Below, the effect of the g_g mode on the APES is analyzed within the $t_{1u}\otimes(g_g\oplus h_g)$ JT model. For simplicity, the index g for parity is omitted in the coupling parameters. Since the g_g mode does not contribute to the D_{5d} deformation, the energy and the JT deformation at the D_{5d} minima are the same as those for the $t_{1u}\otimes h_g$ JT model [39]:

$$U_{D_{5d}} = -\frac{(V^h)^2}{2K^h - \frac{8}{\sqrt{5}}V_1^{hh}}, \tag{6}$$

$$q_{h_g} = \frac{V^h}{K^h - \frac{4}{\sqrt{5}}V_1^{hh}}, \quad q_{g_g} = 0. \tag{7}$$

On the other hand, the energy at the D_{3d} minima is modified by the g_g contribution as

$$U_{D_{3d}} = -\frac{(V^h)^2}{2\left(K^h - \frac{4}{3}V_2^{hh}\right) - \frac{8(V_1^{gh})^2}{9K^g+15V^{gg}}}, \tag{8}$$

$$q_{h_g} = \frac{V^h}{K^h - \frac{4}{3}V_2^{hh} - \frac{4\left(V_1^{gh}\right)^2}{9K^g+15V^{gg}}},$$

$$q_{g_g} = \frac{6V^hV_1^{gh}}{(3K^g+5V^{gg})\left(3K^h-4V_2^{hh}\right) - 4\left(V_1^{gh}\right)^2}. \tag{9}$$

The coupling to the g_g mode lowers the D_{3d} minima. In the case of the D_{2h} minima, two components of h_g and one of g_g become totally symmetric. The analytical expression of the energy at the D_{2h} minima becomes cumbersome, thus approximate forms of U and q, including up to the second-order terms in

quadratic vibronic couplings, are given here:

$$U_{D_{2h}} = -\frac{(V^h)^2}{2K^h}\left[1+\frac{\sqrt{5}V_1^{hh}+9V_2^{hh}}{8K^h} + \frac{3\left(V_1^{gh}\right)^2}{8K^gK^h} + \frac{\left(V_1^{hh}\right)^2+3\left(V_2^{hh}\right)^2}{2(K^h)^2}\right], \tag{10}$$

$$q_{h_g\theta} = \frac{V^h}{K^h}\left[1+\frac{\sqrt{5}V_1^{hh}+9V_2^{hh}}{8K^h} + \frac{3\left(V_1^{gh}\right)^2}{K^gK^h} + \frac{\left(V_1^{hh}\right)^2+3\left(V_2^{hh}\right)^2}{2(K^g)^2}\right],$$

$$q_{h_g\epsilon} = \frac{\sqrt{3}V^h}{8K^h}\left[\frac{3V_1^{hh}-\sqrt{5}V_2^{hh}}{K^h} + \frac{\sqrt{5}V_1^{gh}V_2^{gh}}{K^gK^h}\right],$$

$$q_{g_ga} = \frac{1}{2}\sqrt{\frac{3}{2}}\frac{V^h}{K^h}\left[\frac{V_1^{gh}}{K^g} + \frac{\left(\sqrt{5}V_1^{hh}+9V_2^{hh}\right)V_1^{gh}}{8K^gK^h} + \frac{\left(3\sqrt{5}V_1^{hh}-5V_2^{hh}\right)V_2^{gh}}{8K^gK^h}\right]. \tag{11}$$

The energy difference between the D_{5d} and D_{3d} minima is

$$\Delta U = U_{D_{3d}} - U_{D_{5d}} = \frac{(V^h)^2}{2K^h}\left[\frac{6V_1^{hh}-2\sqrt{5}V_2^{hh}}{3\sqrt{5}K^h} - \frac{2\left(V_1^{gh}\right)^2}{9K^gK^h} + \frac{8\left(V_1^{hh}\right)^2}{5(K^h)^2} + \frac{5\left(V_2^{hh}\right)^2}{9(K^h)^2}\right]. \tag{12}$$

The terms up to the second order of quadratic couplings are taken into account. Considering the usual situation in which $|V^{\Gamma_1\Gamma_2}| < |K^\Gamma|$, the effect of the g_g mode on the APES would be minor.

In the case of $n = 2$–4, the quadratic coupling becomes a few times stronger than that in $n = 1,5$. Due to the presence of the multiplet splitting, the structure of the APES becomes more complicated [61]. The symmetry of the potential minima for $n = 2,4$ is D_{5d}, D_{3d}, or D_{2h} within the $t_{1u}^{2/4} \otimes h_g$ JT model. Therefore, the JT inactive g_g modes would play a similar role as for $n = 1,5$. On the other hand, the potential minimum of the $t_{1u}^3 \otimes h_g$ JT model is either D_{2h} or C_{2h}, and in the latter, t_{1g} and t_{2g} as well as g_g vibrations can modify the APES. For $n = 2$–4, we will not analyze the APES further.

C. Vibronic states

The quadratic vibronic coupling modifies the vibronic states. As discussed in the previous section, the effect of the non-JT modes is expected to be weak, thus only the JT active h_g modes are taken into account here. The nature of the linear vibronic states of the dynamical JT Hamiltonian,

$$\hat{H}^{(0)} = \hat{H}_{\rm bi} + \hat{H}_{\rm vib} + \hat{H}_{\rm JT}^{(1)}, \tag{13}$$

has been intensively studied. Because of the SO(3) symmetry of the linear $T_{1u} \otimes h_g$ JT Hamiltonian [55,63], the Hamiltonian, one of the vibronic angular momenta, $\hat{J}_z$, and the square of the angular momentum, $\hat{\boldsymbol{J}}^2 = \hat{J}_x^2 + \hat{J}_y^2 + \hat{J}_z^2$, are of commuting observables. In addition, in the case of $C_{60}{}^{3-}$, the seniority of the electronic terms [64] is inherited in the vibronic state and expressed by parity [26,58]:

$$\hat{P} = (\hat{I}_{T_{1u}} - \hat{I}_{H_u})\prod_{\mu=1}^{8}\prod_{\gamma=\theta,\epsilon,\xi,\eta,\zeta}(-1)^{\hat{n}_{h_g(\mu)\gamma}}. \tag{14}$$

Here, $\hat{I}_\Gamma$ is the projection operator into the Γ electronic term ($\Gamma = T_{1u}, H_u$), and $\hat{n}_{h_g(\mu)\gamma}$ is the $h_g(\mu)\gamma$ vibrational quantum number operator. Therefore, the linear vibronic states of $C_{60}{}^{n-}$ ($n = 1,2,4,5$) are characterized by the magnitude of the angular momentum J (=0,1,2, ...), its z component M_J (=$-J, -J+1, \ldots, J$), and the principal quantum number α, which distinguishes the energy levels. In the case of $C_{60}{}^{3-}$, parity P (=±1) is added to the set of quantum numbers.

The total angular momenta do not commute with the quadratic vibronic Hamiltonian, $\hat{H}_{\rm JT}^{(2)}$. Thus, the degeneracy of linear vibronic states is partly lifted, and split vibronic states are characterized by the irrep of the I_h group. In the case of $C_{60}{}^{3-}$, the parity (14) does not commute with $\hat{H}_{\rm JT}^{(2)}$:

$$\hat{P}\hat{H}_{\rm JT}^{(2)}\hat{P} = -\hat{H}_{\rm JT}^{(2)}. \tag{15}$$

The vibronic states of the full Hamiltonian,

$$\hat{H} = \hat{H}^{(0)} + \hat{H}_{\rm JT}^{(2)}, \tag{16}$$

are expressed by the superposition of the linear vibronic states. To describe the vibronic states of $\hat{H}$, it is convenient to use the irreducible linear vibronic states, $|\Psi_{\alpha J\Gamma\gamma(P)}^{(0)}\rangle$, where Γ is an irrep included in $J \downarrow I_h$, and γ is a component of Γ. The vibronic states are written

$$|\Psi_{\alpha\Gamma\gamma}\rangle = \sum_{\beta J(P)}\left|\Psi_{\beta J\Gamma\gamma(P)}^{(0)}\right\rangle C_{\beta J\Gamma\gamma(P);\alpha}. \tag{17}$$

Coefficients $C_{\beta J\Gamma\gamma(P);\alpha}$ are determined from the diagonalization of the $\hat{H}$ matrix on the basis of $|\Psi_{\alpha J\Gamma\gamma(P)}^{(0)}\rangle$. There are two selection rules for the matrix elements of $\hat{H}_{\rm JT}^{(2)}$. First, since $\hat{H}_{\rm JT}^{(2)}$ is totally symmetric, the off-diagonal blocks between different irreps are zero. Second, in the case of $C_{60}{}^{3-}$, due to Eq. (15), only the off-diagonal blocks between the $|\Psi_{\alpha J\Gamma\gamma P}^{(0)}\rangle$'s characterized by the opposite parities are nonzero. Accordingly, we have

$$\left\langle\Psi_{\beta J\Gamma\gamma(P)}^{(0)}\middle|\hat{H}_{\rm JT}^{(2)}\middle|\Psi_{\beta' J'\Gamma'\gamma'(P')}^{(0)}\right\rangle = \delta_{\Gamma\Gamma'}\delta_{\gamma\gamma}(\delta_{P,-P'})\left\langle\Psi_{\beta J\Gamma\gamma(P)}^{(0)}\middle|\hat{H}_{\rm JT}^{(2)}\middle|\Psi_{\beta' J'\Gamma\gamma(-P)}^{(0)}\right\rangle. \tag{18}$$

Here, the expressions in parentheses are only considered for $C_{60}{}^{3-}$. Thus, the vibronic levels of $n = 1,2,4,5$ ($n = 3$) change linearly (quadratically) with the strength of the quadratic vibronic coupling.

III. DFT CALCULATIONS OF QUADRATIC VIBRONIC COUPLING PARAMETERS

To derive the quadratic vibronic coupling parameters, the DFT method with a hybrid B3LYP exchange correlation functional [65] and a triple-zeta basis set [6-311G(d)] was employed. All DFT calculations were done using the GAUSSIAN 16 program [66]. The linear orbital vibronic coupling parameters

of C_{60}^- calculated by the hybrid B3LYP functional are close to the experimental data [10]. The electron affinity derived with the Delta-SCF approach to C_{60}^- and C_{60} is 2.497 eV, which is in line with the recent experimental value 2.683 eV [13,51].

The quadratic vibronic coupling constants were derived within three approaches:

(i) Fitting of the APES of deformed C_{60}^- to the model JT Hamiltonian.

(ii) Fitting of the t_{1u} LUMO level of deformed neutral C_{60} to the model JT Hamiltonian.

(iii) Comparing the Hessian for the relaxed C_{60}^- structure and for the model JT Hamiltonian.

In the first approach, the APES of deformed C_{60}^- along various modes are fitted to the quadratic JT Hamiltonian. The deformations are both along the single a_g/h_g mode and also linear combinations of two modes (a_g and h_g or two different h_g). This approach uses the symmetry-broken electronic wave functions, which allows us to take into account the electron correlation; however, artificial error might be introduced. The linear vibronic coupling parameters of C_{60}^- were derived by a similar method using the gradient of the APES at the high-symmetric structure in Ref. [10]. The second method is similar to the first one but with the use of the t_{1u} LUMO of neutral C_{60}. The advantage of the method is that the obtained parameters are free from the artificial error due to the symmetry breaking of the wave function, whereas the effect of the relaxation of the molecular orbitals by electron doping is neglected. As seen in the previous studies on the linear vibronic coupling parameters, the coupling parameters from method (i) [10] and method (ii) [47,49] do not differ much in prediction. In the last approach, the quadratic coupling parameters are derived from the Hessian at the JT deformed structure, since the Hessian at the equilibrium high-symmetric structures contains not only K^Γ but also $V^{\Gamma_1\Gamma_2}$ (Appendix B). By comparing the expression of the second derivatives within the model and the DFT-derived Hessian at the corresponding potential minima, the parameters can be determined. In this work, the Hessians at the D_{2h} and D_{3d} minima were used (the latter is only for V^{gg}). The third approach can provide coupling parameters with a much smaller amount of calculations compared with methods (i) and (ii), nonetheless the relaxed structures might be local minima. In addition to the expectation value of the quadratic vibronic operator, the pseudo JT effect may make an important contribution to the quadratic coupling parameters [67]. In the present approach, the latter is also included in the obtained quadratic coupling parameters because the first-principles APES should contain it.

The derived Hessian and the vibronic coupling constants are tabulated in the supplemental material [53] (Tables S6–S8). The order of the quadratic vibronic coupling parameters is at most 10^{-7} a.u., which is about 10–100 times smaller than K^Γ. Therefore, as seen from Eqs. (6), (8), and (10), the warping of the APES is small in comparison with the linear JT stabilization energy. The influence of the g_g modes on the APES (12) is very small, nonetheless there are small contributions to the deformation [53]. Although the DFT calculations were carefully performed with a fine grid and tight conditions for the convergence of self-consistent-field calculations (highest accuracy within the code [66]), the values of the quadratic coupling parameters depend on approaches (i)–(iii). Given the smallness of the obtained parameters, more accurate calculations would be necessary for the derivation of the reliable quadratic vibronic coupling parameters.

TABLE I. The JT stabilization energies of C_{60}^- with respect to the symmetrized distortions (meV). The origin of the energy corresponds to that of the undeformed structure. (i)–(iii) indicate the methods described in Sec. III.

	(i)	(ii)	(iii)
D_{5d}	−47.06	−49.38	−48.00
D_{3d}	−48.88	−48.44	−48.49
D_{2h}	−48.56	−48.58	−48.40

IV. QUADRATIC JAHN-TELLER EFFECT IN C_{60}^{n-} ANIONS

A. Adiabatic potential energy surface

With the obtained three sets of vibronic parameters, the warping of the APES of C_{60}^- is analyzed. The space for the analysis of the APES's of the $T_{1u} \otimes 8h_g$ JT model can be significantly reduced by employing the symmetrized distortions (Appendix A). The obtained energies are shown in Table I. In the case of parameters (i) and (iii), the D_{3d} minima are more stable than those of D_{5d} and vice versa for (ii). Thus, we cannot conclude about the symmetry of the JT deformation at the global minima as well as the stabilization energy. However, the energy difference between these extrema is less than 2 meV, which is much smaller than the JT stabilization energy of ∼50 meV for C_{60}^-.

The JT distortion of C_{60}^- has been intensively investigated computationally in the past. Our result shows that the D_{5d} minima are more stable by 0.31 meV than the D_{3d} minima. The result disagrees with some of the previous calculations. Within semiempirical modified intermediate neglect of differential overlap (MINDO) [68] and the generalized gradient approximation (GGA) [11], the D_{3d} minima were concluded to be the lowest. Within the unrestricted Hartree-Fock (HF) calculations, the D_{3d} and D_{2h} minima have the same energies, and both are lower than the D_{5d} minima by 0.2 meV [69]. Previous B3LYP calculations also predict the D_{3d} as the global minima, albeit not very reliably because the reported energy gap between the D_{3d} and D_{5d} minima is as much as 40 meV [47]. Our calculations show that the D_{5d} minima reported in Ref. [47] are not the lowest ones. Recent calculations within the local density approximation (LDA) predicted that the D_{2h} minima are more stable than the D_{3d} and D_{5d} minima by 0.5 and 1.5 meV, respectively [70] (the D_{3d} minima are unstable and the global C_{2h} symmetric minima are lower by 0.6 meV and exist close to D_{3d}). However, the order of the D_{5d}, D_{3d}, and D_{2h} minima disagrees with that expected for the $T_{1u} \otimes h_g$ Jahn-Teller model [39].

Finding the global minima of C_{60}^- with first-principles calculations is not an easy task because of the presence of many local minima in the APES. However, taking into account also the previous calculations, D_{3d} minima seem to correspond to the global ones. Compared to the DFT/HF calculations, our estimate of the warping of 2 meV could be regarded as the upper limit.

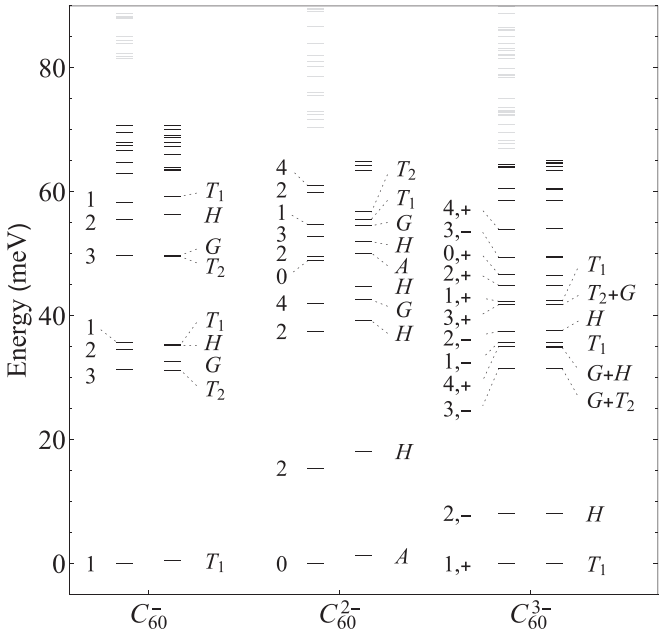

FIG. 1. Vibronic levels without and with quadratic vibronic coupling (meV). For each anion, the linear (left) and quadratic (right) vibronic levels are shown. Among linear vibronic levels, black (light gray) lines show the vibronic levels, which are (not) taken into account to calculate the quadratic vibronic levels. The quadratic coupling parameters obtained with method (i) are used. The vibronic levels are shown with respect to the ground linear vibronic level for each anion.

B. Vibronic states

The vibronic states of C_{60} anions were calculated using the DFT-derived coupling parameters. Using the linear vibronic states presented in Ref. [58], the matrix elements of $\hat{M}^{\Gamma_1\Gamma_2}_{\nu\mu_1\mu_2} = \partial \hat{H}^{(2)}_{\rm JT}/\partial V^{\Gamma_1\Gamma_2}_{\nu\mu_1\mu_2}$ were calculated. The calculated elements are listed in Tables S10–S12 in the supplemental material [53], and hence one can calculate the low-lying vibronic states with other sets of quadratic coupling parameters. Figure 1 shows the linear vibronic levels from Ref. [58] and the obtained vibronic levels with the parameter set (i). The latter is chosen because it gives the largest change in vibronic levels among the three sets of parameters and also it gives the D_{3d} global minima (for other cases, see [53]).

The vibronic levels of $C_{60}{}^{-}$ are shifted at most by 1–2 meV. The shift is enhanced in $C_{60}{}^{2-}$ as expected. However, in both cases, the shift of levels is much smaller than the energy gap between the ground and low-lying vibronic levels. In addition to the weak quadratic vibronic coupling, the vibronic reduction of the matrix elements of $\hat{M}^{\Gamma_1\Gamma_2}_{\nu\mu_1\mu_2}$ further quenches the effect of the quadratic coupling. In the case of $C_{60}{}^{3-}$, the quadratic vibronic coupling changes the vibronic energy quadratically [Eq. (18)], resulting in a very small shift.

As shown above, in all $C_{60}{}^{n-}$ anions the vibronic states are not modified much by the quadratic coupling. Thus, except for the molecular spectroscopic studies with very high resolution, the linear vibronic states are sufficient to quantitatively understand the properties of C_{60} anions. This also means that the JT dynamics of free C_{60} anions is closer to the pseudorotational type than to the tunneling dynamics type. Although the dynamical JT effect is influenced by the environments, in cubic trivalent fullerides the JT dynamics remains of pseudorotational type because of the strong linear JT stabilization and the negligible effect of quadratic vibronic coupling. The higher-order vibronic coupling may play an important role in the study of high-resolution spectroscopy and may also be enhanced in a low-symmetric environment. In the former, the quadratic coupling governs the splitting pattern of the highly degenerate excited vibronic levels (Fig. 1). In the latter, the JT dynamics can be modified in a low-symmetric environment such as solution [9,14], matrix [4,5,11], and surface [24,62]. A quantitative understanding of these situations is beyond the scope of this work.

V. CONCLUSION

We studied the quadratic JT effect of $C_{60}{}^{n-}$ anions (n = 1–5) based on DFT calculations. The main results are the following:

(i) Analysis of the APES of the $T_{1u} \otimes (g_g \oplus h_g)$ JT model.

(ii) Derivation of the selection rules for the matrix elements of the quadratic vibronic contribution on the basis of the linear vibronic states.

(iii) Calculation of the matrix elements of $\hat{H}^{(2)}_{\rm JT}$ on the basis of linear vibronic states.

(iv) DFT derivation of the quadratic orbital vibronic coupling constants of C_{60} anions.

(v) Evaluation of the effect of the quadratic coupling on the low-lying vibronic levels.

Although the DFT-derived quadratic vibronic coupling parameters are not sufficiently accurate, it was revealed that the quadratic coupling has a much weaker effect than the linear vibronic couplings do in $C_{60}{}^{n-}$ anions. Because of the symmetry and vibronic reduction as well as the weak quadratic vibronic couplings, the linear vibronic states of C_{60} anions are not modified much. In particular, the effect of the quadratic coupling is significantly reduced in $C_{60}{}^{3-}$, resulting in robust pseudorotational vibronic dynamics in alkali-doped fullerides. In addition, the effect of the JT inactive g_g modes on the APES was analyzed. The contribution from the g_g mode to the APES is negligible in C_{60} anions, while it could be more important in icosahedral metal clusters where quadratic coupling is expected to be stronger [71,72].

ACKNOWLEDGMENTS

D.L. gratefully acknowledges funding by the China Scholarship Council. N.I. is supported by Japan Society for the Promotion of Science Overseas Research Fellowship.

APPENDIX A: SYMMETRIZED DISPLACEMENT

The JT deformations, which maintain the symmetry of a subgroup G of I_h, are given here ($G = D_{5d}, D_{3d}, D_{2h}$). The expression of the symmetrized h_g displacements has been presented in Refs. [39,61,73]. The following symmetrized displacements contain those by g_g modes as well as the h_g displacements. The pattern of the deformations can be obtained by using the relation between the spherical harmonics and

polynomials: Substituting the direction of the C_5, C_3, and C_2 axes in the Cartesian coordinate (t_{1u} representation) into the spherical harmonics of second rank, the five components of the spherical harmonics correspond to the patterns of symmetrized h_g deformation. The symmetrized g_g deformation is obtained by combining the similar procedure and the relation between the fourth-rank spherical harmonics and $G_g \oplus H_g$. Below, we choose the deformation that keeps the symmetry axes in the zx plane, and the a_g contributions are not explicitly written because they do not lower the symmetry.

Under $I_h \downarrow D_{5d}$, the g_g and h_g representations are reduced as [57]

$$\begin{aligned} g_g \downarrow D_{5d} &= e_{1g} \oplus e_{2g}, \\ h_g \downarrow D_{5d} &= a_g \oplus e_{1g} \oplus e_{2g}. \end{aligned} \tag{A1}$$

Thus, the D_{5d} distortion can be expressed by using one coordinate for each $h_g(\mu)$ mode:

$$\begin{aligned} \Delta \boldsymbol{R}_{D_{5d}} = \frac{1}{\sqrt{M}} \sum_{\mu=1}^{8} q_{h_g(\mu)} \Bigg[& \frac{\phi^2}{2\sqrt{5}} \boldsymbol{e}_{h_g(\mu)\theta} \\ & + \frac{\phi^{-1}}{2} \sqrt{\frac{3}{5}} \boldsymbol{e}_{h_g(\mu)\epsilon} + \sqrt{\frac{3}{5}} \boldsymbol{e}_{h_g(\mu)\eta} \Bigg]. \end{aligned} \tag{A2}$$

Here, M is the mass of a carbon atom. On the other hand, under $I_h \downarrow D_{3d}$, both the g_g and h_g representations contain the totally symmetric representation [57]:

$$\begin{aligned} g_g \downarrow D_{3d} &= a_{1g} \oplus a_{2g} \oplus e_g, \\ h_g \downarrow D_{3d} &= a_{1g} \oplus 2e_g. \end{aligned} \tag{A3}$$

Therefore, the D_{3d} deformation is expressed by one g_g and one h_g coordinate [57]:

$$\begin{aligned} \Delta \boldsymbol{R}_{D_{3d}} = \frac{1}{\sqrt{M}} \sum_{\mu=1}^{8} q_{h_g(\mu)} \Bigg[& -\frac{\phi^{-1}}{2} \boldsymbol{e}_{h_g(\mu)\theta} \\ & + \frac{\phi^2}{2\sqrt{3}} \boldsymbol{e}_{h_g(\mu)\epsilon} + \frac{1}{\sqrt{3}} \boldsymbol{e}_{h_g(\mu)\eta} \Bigg] \\ + \frac{1}{\sqrt{M}} \sum_{\mu=1}^{6} q_{g_g(\mu)} & \left[\frac{1}{\sqrt{6}} \boldsymbol{e}_{g_g(\mu)a} - \sqrt{\frac{5}{6}} \boldsymbol{e}_{g_g(\mu)y} \right]. \end{aligned} \tag{A4}$$

Finally, under $I_h \downarrow D_{2h}$,

$$\begin{aligned} g_g \downarrow D_{2h} &= a_g \oplus b_{1g} \oplus b_{2g} \oplus b_{3g}, \\ h_g \downarrow D_{2h} &= 2a_g \oplus b_{1g} \oplus b_{2g} \oplus b_{3g}. \end{aligned} \tag{A5}$$

Therefore, the g_g and h_g deformations are expressed by one ($q_{g_g a}$) and two ($q_{h_g\theta}$,$q_{h_g\epsilon}$) coordinates, respectively:

$$\begin{aligned} \Delta \boldsymbol{R}_{D_{2h}} = \frac{1}{\sqrt{M}} \sum_{\mu=1}^{8} & [q_{h_g(\mu)\theta} \boldsymbol{e}_{h_g(\mu)\theta} + q_{h_g(\mu)\epsilon} \boldsymbol{e}_{h_g(\mu)\epsilon}] \\ & + \frac{1}{\sqrt{M}} \sum_{\mu=1}^{6} q_{g_g(\mu)a} \boldsymbol{e}_{g_g(\mu)a}. \end{aligned} \tag{A6}$$

In the above equations, $\Delta \boldsymbol{R}_G$ is the 180-dimensional vector consisting of all Cartesian coordinates of carbon atoms in C_{60}, $\boldsymbol{e}_{\Gamma(\mu)\gamma}$ is the polarization vector, $q_{\Gamma(\mu)}$ is the magnitude of the displacement, and $\phi = (1+\sqrt{5})/2$.

APPENDIX B: DERIVATIVES OF THE APES

The second derivatives of the APES with respect to a_g, g_g, and h_g coordinates are given. Below, the APES around the minima with symmetry G is written as U_G ($G = D_{5d}, D_{3d}, D_{2h}$). The notation of the coordinates is the same as in Eqs. (A2), (A4), and (A6). At the D_{5d} structure,

$$\begin{aligned} & \frac{\partial^2 U_{D_{5d}}}{\partial q_{a_g(\mu_1)} \partial q_{a_g(\mu_2)}} = K^{a_g}_{\mu_1\mu_2}, \quad \frac{\partial^2 U_{D_{5d}}}{\partial q_{a_g(\mu_1)} \partial q_{h_g(\mu_2)}} = \frac{1}{2} V^{a_g h_g}_{\mu_1\mu_2}, \\ & \frac{\partial^2 U_{D_{5d}}}{\partial q_{h_g(\mu_1)} \partial q_{h_g(\mu_2)}} = K^{h_g}_{\mu_1\mu_2} + \frac{2}{\sqrt{5}} V^{h_g h_g}_{1\mu_1\mu_2}. \end{aligned} \tag{B1}$$

At the D_{3d} structure,

$$\begin{aligned} & \frac{\partial^2 U_{D_{3d}}}{\partial q_{a_g(\mu_1)} \partial q_{a_g(\mu_2)}} = K^{a_g}_{\mu_1\mu_2}, \quad \frac{\partial^2 U_{D_{3d}}}{\partial q_{a_g(\mu_1)} \partial q_{h_g(\mu_2)}} = -V^{a_g h_g}_{\mu_1\mu_2}, \\ & \frac{\partial^2 U_{D_{3d}}}{\partial q_{g_g(\mu_1)} \partial q_{g_g(\mu_2)}} = K^{g_g}_{\mu_1\mu_2} + \frac{5}{3} V^{g_g g_g}_{\mu_1\mu_2}, \\ & \frac{\partial^2 U_{D_{3d}}}{\partial q_{g_g(\mu_1)} \partial q_{h_g(\mu_2)}} = -\frac{2}{3} V^{g_g h_g}_{1\mu_1\mu_2}, \\ & \frac{\partial^2 U_{D_{3d}}}{\partial q_{h_g(\mu_1)} \partial q_{h_g(\mu_2)}} = K^{h_g}_{\mu_1\mu_2} - \frac{4}{3} V^{h_g h_g}_{2\mu_1\mu_2}. \end{aligned} \tag{B2}$$

At the D_{2h} structure,

$$\begin{aligned} & \frac{\partial^2 U_{D_{2h}}}{\partial q_{a_g(\mu_1)} \partial q_{a_g(\mu_2)}} = K^{a_g}_{\mu_1\mu_2}, \quad \frac{\partial^2 U_{D_{2h}}}{\partial q_{a_g(\mu_1)} \partial q_{h_g(\mu_2)}} = -V^{a_g h_g}_{\mu_1\mu_2}, \\ & \frac{\partial^2 U_{D_{2h}}}{\partial q_{g_g(\mu_1)a} \partial q_{g_g(\mu_2)a}} = K^{g_g}_{\mu_1\mu_2}, \\ & \frac{\partial^2 U_{D_{2h}}}{\partial q_{g_g(\mu_1)a} \partial q_{h_g(\mu_2)\theta}} = -\frac{1}{2}\sqrt{\frac{3}{2}} V^{g_g h_g}_{1\mu_1\mu_2}, \\ & \frac{\partial^2 U_{D_{2h}}}{\partial q_{g_g(\mu_1)a} \partial q_{h_g(\mu_2)\epsilon}} = -\frac{1}{2}\sqrt{\frac{5}{2}} V^{g_g h_g}_{2\mu_1\mu_2}, \\ & \frac{\partial^2 U_{D_{2h}}}{\partial q_{h_g(\mu_1)\theta} \partial q_{h_g(\mu_2)\theta}} = K^{h_g}_{\mu_1\mu_2} - \frac{\sqrt{5}}{8} V^{h_g h_g}_{1\mu_1\mu_2} - \frac{9}{8} V^{h_g h_g}_{2\mu_1\mu_2}, \\ & \frac{\partial^2 U_{D_{2h}}}{\partial q_{h_g(\mu_1)\theta} \partial q_{h_g(\mu_2)\epsilon}} = -\frac{3}{8}\sqrt{3} V^{h_g h_g}_{1\mu_1\mu_2} + \frac{\sqrt{15}}{8} V^{h_g h_g}_{2\mu_1\mu_2}, \\ & \frac{\partial^2 U_{D_{2h}}}{\partial q_{h_g(\mu_1)\epsilon} \partial q_{h_g(\mu_2)\epsilon}} = K^{h_g}_{\mu_1\mu_2} + \frac{\sqrt{5}}{8} V^{h_g h_g}_{1\mu_1\mu_2} + \frac{9}{8} V^{h_g h_g}_{2\mu_1\mu_2}. \end{aligned} \tag{B3}$$

[1] H. A. Jahn and E. Teller, Stability of polyatomic molecules in degenerate electronic states. I. Orbital degeneracy, Proc. R. Soc. London, Ser. A **161**, 220 (1937).

[2] I. B. Bersuker and V. Z. Polinger, *Vibronic Interactions in Molecules and Crystals* (Springer-Verlag, Berlin, 1989).

[3] C. C. Chancey and M. C. M. O'Brien, *The Jahn-Teller Effect in* C_{60} *and Other Icosahedral Complexes* (Princeton University Press, Princeton, NJ, 1997).

[4] T. Kato, T. Kodama, and T. Shida, Spectroscopic studies of the radical anion of C_{60}. Detection of the fluorescence and reinvestigation of the ESR spectrum, Chem. Phys. Lett. **205**, 405 (1993).

[5] H. Kondo, T. Momose, and T. Shida, Reinvestigation of the low-lying electronic states of C_{60}^-, Chem. Phys. Lett. **237**, 111 (1995).

[6] O. Gunnarsson, H. Handschuh, P. S. Bechthold, B. Kessler, G. Ganteför, and W. Eberhardt, Photoemission Spectra of C_{60}^-: Electron-Phonon Coupling, Jahn-Teller Effect, and Superconductivity in the Fullerides, Phys. Rev. Lett. **74**, 1875 (1995).

[7] S. Tomita, J. U. Andersen, E. Bonderup, P. Hvelplund, B. Liu, S. B. Nielsen, U. V. Pedersen, J. Rangama, K. Hansen, and O. Echt, Dynamic Jahn-Teller Effects in Isolated C_{60}^- Studied by Near-Infrared Spectroscopy in a Storage Ring, Phys. Rev. Lett. **94**, 053002 (2005).

[8] S. Tomita, J. U. Andersen, H. Cederquist, B. Concina, O. Echt, J. S. Forster, K. Hansen, B. A. Huber, P. Hvelplund, J. Jensen, B. Liu, B. Manil, L. Maunoury, S. Brøndsted Nielsen, J. Rangama, H. T. Schmidt, and H. Zettergren, Lifetimes of C_{60}^{2-} and C_{70}^{2-} dianions in a storage ring, J. Chem. Phys. **124**, 024310 (2006).

[9] I. D. Hands, J. L. Dunn, C. A. Bates, M. J. Hope, S. R. Meech, and D. L. Andrews, Vibronic interactions in the visible and near-infrared spectra of C_{60}^- anions, Phys. Rev. B **77**, 115445 (2008).

[10] N. Iwahara, T. Sato, K. Tanaka, and L. F. Chibotaru, Vibronic coupling in C_{60}^- anion revisited: Derivations from photoelectron spectra and DFT calculations, Phys. Rev. B **82**, 245409 (2010).

[11] B. Kern, D. Strelnikov, P. Weis, A. Böttcher, and M. M. Kappes, IR absorptions of C_{60}^+ and C_{60}^- in neon matrixes, J. Phys. Chem. A **117**, 8251 (2013).

[12] K. Støchkel and J. U. Andersen, Photo excitation and laser detachment of C_{60}^- anions in a storage ring, J. Chem. Phys. **139**, 164304 (2013).

[13] D.-L. Huang, P.-D. Dau, H.-T. Liu, and L.-S. Wang, High-resolution photoelectron imaging of cold C_{60}^- anions and accurate determination of the electron affinity of C_{60}, J. Chem. Phys. **140**, 224315 (2014).

[14] K. Kundu, D. R. Kattnig, B. Mladenova, G. Grampp, and R. Das, Electron spin relaxation of C_{60} monoanion in liquid solution: Applicability of Kivelson-Orbach mechanism, J. Phys. Chem. A **119**, 3200 (2015).

[15] O. Gunnarsson, Superconductivity in fullerides, Rev. Mod. Phys. **69**, 575 (1997).

[16] O. Gunnarsson, *Alkali-Doped Fullerides: Narrow-Band Solids with Unusual Properties* (World Scientific, Singapore, 2004).

[17] A. Auerbach, N. Manini, and E. Tosatti, Electron-vibron interactions in charged fullerenes. I. Berry phases, Phys. Rev. B **49**, 12998 (1994).

[18] N. Manini, E. Tosatti, and A. Auerbach, Electron-vibron interactions in charged fullerenes. II. Pair energies and spectra, Phys. Rev. B **49**, 13008 (1994).

[19] M. C. M. O'Brien, Vibronic energies in $C_{60}{}^{n-}$ and the Jahn-Teller effect, Phys. Rev. B **53**, 3775 (1996).

[20] J. Winter and H. Kuzmany, Landau damping and lifting of vibrational degeneracy in metallic potassium fulleride, Phys. Rev. B **53**, 655 (1996).

[21] V. Brouet, H. Alloul, T.-N. Le, S. Garaj, and L. Forró, Role of Dynamic Jahn-Teller Distortions in Na_2C_{60} and Na_2CsC_{60} Studied by NMR, Phys. Rev. Lett. **86**, 4680 (2001).

[22] V. Brouet, H. Alloul, S. Garaj, and L. Forró, Persistence of molecular excitations in metallic fullerides and their role in a possible metal to insulator transition at high temperatures, Phys. Rev. B **66**, 155124 (2002).

[23] L. F. Chibotaru, Spin-Vibronic Superexchange in Mott-Hubbard Fullerides, Phys. Rev. Lett. **94**, 186405 (2005).

[24] A. Wachowiak, R. Yamachika, K. H. Khoo, Y. Wang, M. Grobis, D.-H. Lee, S. G. Louie, and M. F. Crommie, Visualization of the molecular Jahn-Teller effect in an insulating K_4C_{60} monolayer, Science **310**, 468 (2005).

[25] G. Klupp, P. Matus, K. Kamarás, A. Y. Ganin, A. McLennan, M. J. Rosseinsky, Y. Takabayashi, M. T. McDonald, and K. Prassides, Dynamic Jahn-Teller effect in the parent insulating state of the molecular superconductor Cs_3C_{60}, Nat. Commun. **3**, 912 (2012).

[26] N. Iwahara and L. F. Chibotaru, Dynamical Jahn-Teller Effect and Antiferromagnetism in Cs_3C_{60}, Phys. Rev. Lett. **111**, 056401 (2013).

[27] A. Potočnik, A. Y. Ganin, Y. Takabayashi, M. T. McDonald, I. Heinmaa, P. Jeglič, R. Stern, M. J. Rosseinsky, K. Prassides, and D. Arčon, Jahn-Teller orbital glass state in the expanded fcc Cs_3C_{60} fulleride, Chem. Sci. **5**, 3008 (2014).

[28] N. Iwahara and L. F. Chibotaru, Dynamical Jahn-Teller instability in metallic fullerides, Phys. Rev. B **91**, 035109 (2015).

[29] R. H. Zadik, Y. Takabayashi, G. Klupp, R. H. Colman, A. Y. Ganin, A. Potočnik, P. Jeglič, D. Arčon, P. Matus, K. Kamarás, Y. Kasahara, Y. Iwasa, A. N. Fitch, Y. Ohishi, G. Garbarino, K. Kato, M. J. Rosseinsky, and K. Prassides, Optimized unconventional superconductivity in a molecular Jahn-Teller metal, Sci. Adv. **1**, e1500059 (2015).

[30] N. Iwahara and L. F. Chibotaru, Orbital disproportionation of electronic density is a universal feature of alkali-doped fullerides, Nat. Commun. **7**, 13093 (2016).

[31] Y. Nomura, S. Sakai, M. Capone, and R. Arita, Exotic *s*-wave superconductivity in alkali-doped fullerides, J. Phys.: Condens. Matter **28**, 153001 (2016).

[32] A. Nava, C. Giannetti, A. Georges, E. Tosatti, and M. Fabrizio, Cooling quasiparticles in A_3C_{60} fullerides by excitonic mid-infrared absorption, Nat. Phys. **14**, 154 (2018).

[33] Y. Matsuda, N. Iwahara, K. Tanigaki, and L. F. Chibotaru, arXiv:1805.07753.

[34] T. Kawamoto, A theoretical model for ferromagnetism of TDAE-C_{60}, Solid State Commun. **101**, 231 (1997).

[35] T. Sato, T. Yamabe, and K. Tanaka, Magnetic ordering in fullerene charge-transfer complexes, Phys. Rev. B **56**, 307 (1997).

[36] K. Yu. Amsharov, Y. Krämer, and M. Jansen, Direct observation of the transition from static to dynamic Jahn-Teller effects in the $[Cs(THF)_4]C_{60}$ fulleride, Angew. Chem. Int. Ed. **50**, 11640 (2011).

[37] E. A. Francis, S. Scharinger, K. Németh, K. Kamarás, and C. A. Kuntscher, Pressure-induced transition from the dynamic to static Jahn-Teller effect in $(Ph_4P)_2IC_{60}$, Phys. Rev. B **85**, 195428 (2012).

[38] D. V. Konarev, A. V. Kuzmin, S. V. Simonov, E. I. Yudanova, S. S. Khasanov, G. Saito, and R. N. Lyubovskaya, Experimental observation of C_{60} LUMO splitting in the C_{60}^{2-} dianions due to the Jahn-Teller effect. Comparison with the C_{60}^{-} radical anions, Phys. Chem. Chem. Phys. **15**, 9136 (2013).

[39] J. L. Dunn and C. A. Bates, Analysis of the $T_{1u} \otimes h_g$ Jahn-Teller system as a model for C_{60} molecules, Phys. Rev. B **52**, 5996 (1995).

[40] L. M. Sindi, I. D. Hands, J. L. Dunn, and C. A. Bates, A study of the quadratic $p^2 \otimes h$ Jahn-Teller system, J. Mol. Struct. **838**, 78 (2007).

[41] C. M. Varma, J. Zaanen, and K. Raghavachari, Superconductivity in the fullerenes, Science **254**, 989 (1991).

[42] M. Schluter, M. Lannoo, M. Needels, G. A. Baraff, and D. Tománek, Electron-Phonon Coupling and Superconductivity in Alkali-Intercalated C_{60} Solid, Phys. Rev. Lett. **68**, 526 (1992).

[43] J. C. R. Faulhaber, D. Y. K. Ko, and P. R. Briddon, Vibronic coupling in C_{60} and C_{60}^{3-}, Phys. Rev. B **48**, 661 (1993).

[44] V. P. Antropov, O. Gunnarsson, and A. I. Liechtenstein, Phonons, electron-phonon, and electron-plasmon coupling in C_{60} compounds, Phys. Rev. B **48**, 7651 (1993).

[45] N. Breda, R. A. Broglia, G. Colò, H. E. Roman, F. Alasia, G. Onida, V. Ponomarev, and E. Vigezzi, Electron-phonon coupling in charged buckminsterfullerene, Chem. Phys. Lett. **286**, 350 (1998).

[46] N. Manini, A. Dal Corso, M. Fabrizio, and E. Tosatti, Electron-vibration coupling constants in positively charged fullerene, Philos. Mag. B **81**, 793 (2001).

[47] M. Saito, Electron-phonon coupling of electron- or hole-injected C_{60}, Phys. Rev. B **65**, 220508 (2002).

[48] T. Frederiksen, K. J. Franke, A. Arnau, G. Schulze, J. I. Pascual, and N. Lorente, Dynamic Jahn-Teller effect in electronic transport through single C_{60} molecules, Phys. Rev. B **78**, 233401 (2008).

[49] J. Laflamme Janssen, M. Côté, S. G. Louie, and M. L. Cohen, Electron-phonon coupling in C_{60} using hybrid functionals, Phys. Rev. B **81**, 073106 (2010).

[50] O. Gunnarsson, Strongly correlated electrons: Estimates of model parameters, in *Correlated Electrons: From Models to Materials Modeling and Simulation*, edited by E. Pavarini, E. Koch, F. Anders, and M. Jarrell (Forschungszentrum Jülich GmbH, Jülich, 2012), Vol. 2, Chap. 9.

[51] X.-B. Wang, H.-K. Woo, and L.-S. Wang, Vibrational cooling in a cold ion trap: Vibrationally resolved photoelectron spectroscopy of cold C_{60}^{-} anions, J. Chem. Phys. **123**, 051106 (2005).

[52] C. Faber, J. L. Janssen, M. Côté, E. Runge, and X. Blase, Electron-phonon coupling in the C_{60} fullerene within the many-body GW approach, Phys. Rev. B **84**, 155104 (2011).

[53] See Supplemental Material at http://link.aps.org/supplemental/10.1103/PhysRevB.98.035402 for the definition of normal modes and symmetrized products of nuclear coordinates, orbital vibronic coupling parameters, Hamiltonian matrices, matrix elements of quadratic vibronic coupling, and vibronic levels.

[54] M. C. M. O'Brien, Dynamic Jahn-Teller effect in an orbital triplet state coupled to both E_g and T_{2g} vibrations, Phys. Rev. **187**, 407 (1969).

[55] M. C. M. O'Brien, The Jahn-Teller effect in a p state equally coupled to E_g and T_{2g} vibrations, J. Phys. C **4**, 2524 (1971).

[56] L. L. Boyle and Y. M. Parker, Symmetry coordinates and vibration frequencies for an icosahedral cage, Mol. Phys. **39**, 95 (1980).

[57] S. L. Altmann and P. Herzig, *Point-Group Theory Tables* (Clarendon Press, Oxford, 1994).

[58] D. Liu, N. Iwahara, and L. F. Chibotaru, Dynamical Jahn-Teller effect of fullerene anions, Phys. Rev. B **97**, 115412 (2018).

[59] A. D. Liehr, Topological aspects of the conformational stability problem. Part I. Degenerate electronic states, J. Phys. Chem. **67**, 389 (1963).

[60] S. Muramatsu and T. Iida, A possibility of orthorhombic Jahn-Teller distortion, J. Phys. Chem. Solids **31**, 2209 (1970).

[61] H. S. Alqannas, A. J. Lakin, J. A. Farrow, and J. L. Dunn, Interplay between Coulomb and Jahn-Teller effects in icosahedral systems with triplet electronic states coupled to h-type vibrations, Phys. Rev. B **88**, 165430 (2013).

[62] J. L. Dunn, H. S. Alqannas, and A. J. Lakin, Jahn-Teller effects and surface interactions in multiply-charged fullerene anions and the effect on scanning tunneling microscopy images, Chem. Phys. **460**, 14 (2015).

[63] D. R. Pooler, Continuous group invariances of linear Jahn-Teller systems. II. Extension and application to icosahedral systems, J. Phys. C **13**, 1029 (1980).

[64] G. Racah, Theory of complex spectra. III, Phys. Rev. **63**, 367 (1943).

[65] A. D. Becke, Density-functional thermochemistry. III. The role of exact exchange, J. Chem. Phys. **98**, 5648 (1993).

[66] M. J. Frisch, G. W. Trucks, H. B. Schlegel, G. E. Scuseria, M. A. Robb, J. R. Cheeseman, G. Scalmani, V. Barone, G. A. Petersson, H. Nakatsuji, X. Li, M. Caricato, A. V. Marenich, J. Bloino, B. G. Janesko, R. Gomperts, B. Mennucci, H. P. Hratchian, J. V. Ortiz, A. F. Izmaylov, J. L. Sonnenberg, D. Williams-Young, F. Ding, F. Lipparini, F. Egidi, J. Goings, B. Peng, A. Petrone, T. Henderson, D. Ranasinghe, V. G. Zakrzewski, J. Gao, N. Rega, G. Zheng, W. Liang, M. Hada, M. Ehara, K. Toyota, R. Fukuda, J. Hasegawa, M. Ishida, T. Nakajima, Y. Honda, O. Kitao, H. Nakai, T. Vreven, K. Throssell, J. A. Montgomery, Jr., J. E. Peralta, F. Ogliaro, M. J. Bearpark, J. J. Heyd, E. N. Brothers, K. N. Kudin, V. N. Staroverov, T. A. Keith, R. Kobayashi, J. Normand, K. Raghavachari, A. P. Rendell, J. C. Burant, S. S. Iyengar, J. Tomasi, M. Cossi, J. M. Millam, M. Klene, C. Adamo, R. Cammi, J. W. Ochterski, R. L. Martin, K. Morokuma, O. Farkas, J. B. Foresman, and D. J. Fox, *Gaussian16 Revision A.03* (Gaussian, Inc., Wallingford, CT, 2016).

[67] P. García-Fernández, I. B. Bersuker, J. A. Aramburu, M. T. Barriuso, and M. Moreno, Origin of warping in the $E \bigotimes e$ Jahn-Teller problem: Quadratic vibronic coupling versus anharmonicity and application to $NaCl : Rh^{2+}$ and triangular molecules, Phys. Rev. B **71**, 184117 (2005).

[68] K. Tanaka, M. Okada, K. Okahara, and T. Yamabe, Structure and electronic state of C_{60}^{-}, Chem. Phys. Lett. **193**, 101 (1992).

[69] N. Koga and K. Morokuma, Ab initio MO study of the C_{60} anion radical: The Jahn-Teller distortion and electronic structure, Chem. Phys. Lett. **196**, 191 (1992).

[70] H. Ramanantoanina, M. Gruden-Pavlovic, M. Zlatar, and C. Daul, Density functional theory study of the multimode Jahn-Teller problem in the fullerene anion, Int. J. Quantum Chem. **113**, 802 (2013).

[71] J.-Y. Yi, D. J. Oh, and J. Bernholc, Structural Distortions in Metal Clusters, Phys. Rev. Lett. **67**, 1594 (1991).

[72] S.-Y. Wang, W. Duan, D.-L. Zhao, and C.-Y. Wang, First-principles study of the stability of the icosahedral Ti_{13},Ti_{13}^{-1}, and Ti_{13}^{+1} clusters, Phys. Rev. B **65**, 165424 (2002).

[73] I. D. Hands, J. L. Dunn, W. A. Diery, and C. A. Bates, Vibronic coupling in the icosahedral C_{60}^{2+} Jahn-Teller cation: Repercussions of the nonsimple reducibility of the $H \bigotimes H$ product, Phys. Rev. B **73**, 115435 (2006).